Flywheel-Based Distributed Bus Signalling Strategy for the Public Fast Charging Station

Dragicevic, Tomislav; Sucic, Stepjan; Quintero, Juan Carlos Vasquez; Guerrero, Josep M.

Published in:
I E E E Transactions on Smart Grid

DOI (link to publication from Publisher):
10.1109/TSG.2014.2325963

Publication date:
2014

Document Version
Early version, also known as pre-print

This document is the preprint version of the paper:
T.Dragičević, S. Sučić, J.C. Vasquez, and J. M. Guerrero:
"Flywheel-Based Distributed Bus Signalling Strategy for the Public Fast Charging Station ", IEEE Trans. on Smart Grid, 2014

Flywheel-Based Distributed Bus Signalling Strategy for the Public Fast Charging Station

Tomislav Dragičević, *Member, IEEE,* Stjepan Sučić, *Student Member, IEEE,*, Juan C. Vasquez, *Senior Member, IEEE* Josep M. Guerrero, *Senior Member, IEEE*

***Abstract*—Fast charging stations (FCS) are able to recharge plug-in hybrid electric vehicles (pHEVs) in less than half an hour, thus representing an appealing concept to vehicle owners since the off-road time is similar as for refuelling at conventional public gas stations. However, since these FCS plugs have power ratings of up to 100 kW, they may expose the utility mains to intolerable stresses in the near future scenario where there will be a large number of public FCS spread across the network. This paper proposes an internal power balancing strategy for FCS based on flywheel energy storage system (ESS) which is able to mitigate those impacts by ramping the initial power peak. The balancing strategy was implemented in a distributed manner to grid and flywheel interfacing converters by means of distributed bus signaling (DBS) method. Since the parameters in the proposed upper hierarchical control layer affect the stability features of the system, a reduced order small-signal model has been assembled and parameters have been selected accordingly. Finally, real-time simulation results performed on a full scale model have been reported in order to verify the validity of proposed approach.**

***Index Terms*—Fast charge station (FCS), plug-in hybrid electric vehicle (pHEV), DC-bus signaling (DBS), flywheel.**

I. Introduction

THE transportation sector is currently responsible for one quarter of the world's total carbon dioxide emissions [1]. Its prevalent form is the private road transport which consists of short and long distance journeys realized by means of passenger vehicles, motorcycles and trucks. It currently accounts for 74% of the total transportation pollution, with its share continuing to grow [2]. Since petroleum-based fuels are the main driver of that sector, contributing with more than 95% of the driving energy [3], its greater electrification by introducing the concept of a more electric vehicle (MEV) opens up many possibilities for supporting an on-going utility shift towards cleaner electricity.

Plug-in MEVs are typically split into two categories; plug-in electric vehicles (pEVs) and plug-in hybrid electric vehicles (pHEVs). PEV is powered entirely by an electric engine, while the propulsion of pHEV is resolved by a combination of the electric and internal combustion engine (ICE). Taking into account the current prices of fossil fuels and lithium-ion (Li-Ion) batteries, the most commonly used battery technology in vehicular appliances, pHEVs are currently much more cost-effective than pEVs [4]. Since they are expected to play a significant role in the overall workload of future distribution networks, a creation of appropriate surroundings for the acceptance of their fleets is one of the most important smart grid (SG) objectives. The prevailing concern in that sense is the combined impact of a large number of randomly connected pHEV chargers on the distribution network [5]–[7].

In accordance with the associated grid interface and supported charge rate, three charging levels for electric vehicles may be defined [8]; 1) Regular household single phase AC plug that supports power of up to 2 kW 2) Dedicated AC plug that supports power from 6.6 up to 19.2 kW 3) Dedicated DC plug with built-in charger that has virtually no limit on charging power, with currently available products ranging up to 100 kW. It is predicted that the overall future HEV charging infrastructure will consist of all of the above described technologies. In this respect, level 1 and 2 will generally be more appropriate for applications where recharging duration is not of critical importance, i.e. household and commercial building installations. On the other hand, fast level 3 recharging will be used in public installation sites such as today's gas stations.

This paper deals with the design of a public fast charging station (FCS). Two types of adverse effects associated with the grid interface of FCS may be distinguished; 1) High power shock at the moment of vehicle connection and 2) High power stretch over a period of time. Thus, a large number of FCS may appear as a significant disturbance to the grid in its basic form. Furthermore, it reduces the equivalent spinning reserve of the system, thus increasing the possibility of frequency collapse since the intersection of the power system load and generation characteristic is shifted closer to the unstable region [9]. Finally, the peak loading of the system will be inevitably increased, eventually leading up to overload of some corridors of the transmission and/or distribution network [10]–[12].

In order to deal with aforementioned issues, a vehicle to grid (V2G) concept has emerged as a possibility where aggregated batteries of grid-connected vehicles serve as a bulk energy storage that is able to support the grid operation [13], [14]. However, this strategy implies violation of the recommended charging pattern, which causes accelerated wear and tear of the batteries, thus reducing their lifetime and performance. Taking into account the current battery technology, it seems that this strategy will for a while remain only in academic discussions [15].

Other approaches propose application of an independent energy storage system (ESS) to a common DC link, hence creating a power buffer which can supply a portion of charging power [16], [17]. However, authors in [16] consider direct connection of the dedicated battery pack which causes unregulated DC link voltage deviations as the respective battery gets charged and discharged. Furthermore, degradation is a well-known pitfall of using BESS for prolonged periods of

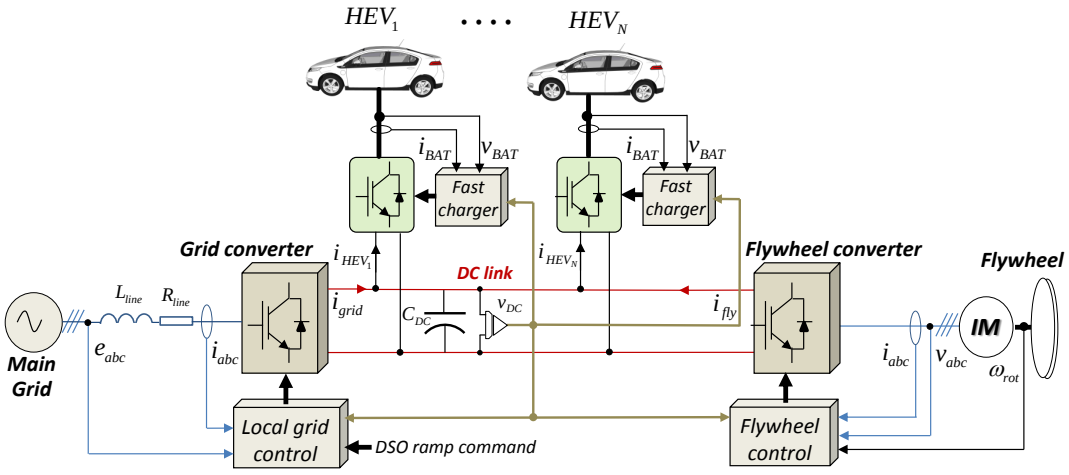

Fig. 1. Diagram of a pHEV fast charging station.

time in aggressive environments (high current peaks, frequent cycling). Considering potentially a high number of vehicles being recharged at the station on a daily basis, even the most advanced BESS will suffer from accelerated capacity and performance loss, which will finally be projected to reduced reliability of the system. Since the technology for estimation of BESS state of health has still not reached a sufficient level of maturity, accurate reliability assessment of such applications is an open issue [18]. On the other hand, electric double layer capacitor (EDLC) which has significantly higher cycle life, is processed through power electronic interface in [17]. However, the cost of EDLC limits its applicability to systems that require peak power for several tens of seconds only [19], [20]. Therefore, EDLC systems are typically designed with very low energy density and are much more appropriate for compensating quick power peaks than for gradual ramping of disturbance [21].

In this paper, a low-speed flywheel ESS driven by an induction machine (IM) is used for internal power balancing purposes as it is an established, rugged and cheap technology that perfectly suits moderate energy and high power density requirements and also supports for large number of charge/discharge cycles. It has been extensively used in past for DC-link coupled power balancing in grid-connected applications [22]–[25]. However, in all of these applications, a high bandwidth communication between the flywheel converter (FC) and grid converter (GC) was needed since the supervisory controller was centralized. On the contrary, this paper uses DC bus voltage as a principal communication medium and distributed bus signaling (DBS) strategy, commonly used for control of DC microgrids [26]–[28] has been applied for the purpose of internal power coordination between units.

The paper is organized as follows. Section II reveals the configuration of FCS and develops a dynamic model for every individual component of the system. In Section III, a DBS method is proposed to achieve decentralized coordination between all units and the full scale control architecture used for real-time simulations is presented. Also, the principle of calculating required flywheel inertia taking into account the possible number of connected HEVs and their charging patterns is given. In Section IV, a reduced order small-signal stability model which incorporates the control loops related with DBS is assembled in order to study its effect on system dynamics and select the viable DBS parameter values. Real-time power hardware in the loop (PHiL) simulation results that indicate the advantages of proposed method with respect to conventional approach are presented in Section V. Finally, Section VI gives the conclusion.

II. Configuration of a DC Fast Charge Station

Diagram of a FCS, formed around the common DC bus, is depicted in Fig. 1. The corresponding power electronic architecture comprises a set of DC/DC converters that serve as HEV chargers and a pair of three-phase full bridge AC/DC converters, one of which is used as a grid interface while the other provides a variable speed operation of the flywheel. The nominal voltage of the common DC bus was selected to be 650 VDC, since it allows complete recharge of all commercially available HEV batteries with basic buck converter topology [4].

By inspecting the system diagram shown in Fig. 1, one may derive the dynamic representation of the system according to current balance in DC-link capacitor

$$C_{DC}\frac{dv_{DC}}{dt} = i_{grid} + i_{fly} - i_{HEV} \tag{1}$$

where C_{DC} is the capacitance connected to the bus, i_{grid} and i_{fly} are the DC currents flowing from the grid and flywheel, respectively, while i_{HEV} is the current extracted by the fast DC charger(s) defined as

$$i_{HEV} = \sum_{j=1}^{N} i_{HEV_j} \tag{2}$$

Only a single HEV charger is considered in this paper, but the proposed concept can be extended to more of them without loss of generalization.

Voltage variations in the common DC-link are determined by DC side current injection/extraction of respective units, dynamics of which may be studied independently since they are decoupled by the capacitor in the common bus. Then, the models of individual components should be combined again into (1) in order to obtain the full system model.

With the aim of facilitating the analysis, it was assumed that the converters' switching frequencies are an order of magnitude above the bandwidths of all the current control loops. Hence, averaged models of power electronics stages could have been directly used for analyzing the low frequency dynamics of the system. As already mentioned, three distinctive power processing components may be recognized. Each one of them introduces some specific features to the system, as outlined below:

1) HEV charger; DC/DC converter with integrated HEV battery charging algorithm. The common charging strategy comprises constant current followed by the constant voltage charging (as seen from the HEV battery terminals) and is usually resolved by means of a low bandwidth controller. It is advisable that the battery controller is slow since the current rise time virtually do not influence the overall charging period, but fast current transients have an adverse impact on battery lifetime.
2) Grid interface; AC/DC rectifier, the dynamics of which are determined by the design of grid filter and inner control loops. To that end, the output filter my be a single three-phase inductor [29], or an LCL configuration [30], [31]. In this paper, an L connection is considered.
3) Flywheel ESS; DC/AC bidirectional converter interfaced to a squirrel cage IM. The dynamics of this subsystem are governed by the machine parameters and the settings of associated control loops. Standard field oriented control (FOC) has been considered as it can provide rapid and accurate torque response [32].

In order to analyze the dynamic behavior of the overall system, each of the aforementioned components is picked one at a time and corresponding small signal representations are derived. The results are presented in the following subsections.

A. Hybrid Electric Vehicle Charger

Typical HEV is composed of an autonomous DC electrical distribution system which couples the principal components, i.e. battery pack, electric engine and ICE. Despite the fact that part of the charge to the battery can be replenished by regenerative braking mechanism, the majority is drawn from the external source.

For that purpose, a dedicated power electronic interface normally serves as the power processing stage between the power source and HEV. Unlike in the case of AC plug where the charger is incorporated within the movable vehicle, fast DC chargers have the common DC link accomplished in the charging station. Therefore, dimensioning of this converter is a non-critical issue and much faster recharge rates can be obtained without increasing vehicle's weight.

The charging converter is regulated by the algorithm recommended by HEV battery manufacturer. It typically comprises two stages in case of Li-Ion batteries; constant current followed by the constant voltage charging pattern. The respective set values should comply with those recommended by battery manufacturers not only to preserve the lifetime but also to avoid potential hazardous conditions. In order to have control over both of these set values, a typical algorithm comprises two nested control loops; inner current loop and outer voltage loop [33]. High bandwidth of inner current loop, which is faster of the two, is not of critical importance since it will have a negligible impact on the total recharging period. In fact, as very quick current rise times can have an adverse impact on battery's lifetime, it is preferred to limit the bandwidth of the current loop to only a few rad/s [18], [34].

A standard Thevenin-based model was used for representing the HEV battery. It contains a state-of-charge (SOC) dependent DC voltage source followed by one R element which represents an instantaneous resistance and two parallel RC elements that emulate the battery dynamics [35]. Model in this paper was composed following the same time constants, but with respect to typical HEV discharge curves given in [36]. The time constants of these elements for HEV batteries are normally in order of magnitude of several minutes. Hence the dynamics of control loops can be considered as decoupled from those of battery.

As a consequence of low current loop bandwidth and even slower battery dynamics, the moment of connection of HEV to the common DC bus may be modeled as the step increase of current sink behind the low pass filter. Indeed, any number of chargers may be represented using the same strategy, by adding up contributions of individual chargers into a single current sink.

B. Grid Converter

The inductor voltage balance equations for each symmetrical converter leg of a three-phase GC can be written in continuous form and then subsequently transformed into a d-q synchronous reference frame, resulting in following expression [29]:

$$\begin{bmatrix} \dot{i}_d \\ \dot{i}_q \end{bmatrix} = \frac{v_{DC}}{L_{line}} \begin{bmatrix} d_d \\ d_q \end{bmatrix} + \begin{bmatrix} -\frac{Rline}{L_{line}} & \omega \\ -\omega & -\frac{Rline}{L_{line}} \end{bmatrix} \begin{bmatrix} i_d \\ i_q \end{bmatrix} - \frac{1}{L_{line}} \begin{bmatrix} e_d \\ e_q \end{bmatrix} \tag{3}$$

where i_q and i_d, d_q and d_d are DC-like currents and duty ratios aligned with q and d rotating axes, respectively, while R_{line} and L_{line} are per phase resistance and inductance of the AC line.

The duty ratios d_d and d_q are generated first by passing the current errors through associated PI regulators. Then the cross-coupling terms are canceled with appropriate feed-forward compensation and the result is divided with v_{DC} in order to remove non-linearities in the first term of (3). Now, the regulation of currents in d and q axis is decoupled and it does not depend upon variations of v_{DC}. As a matter of fact, since the structure of both axes is equivalent, settings of their PI controllers should be the same as well. To that end, the proportional and integral terms can be tuned to cancel the dominant pole introduced by the $L_{line} \cdot s + R_{line}$ element

making each axis to behave as a first order delay with the respective time constant being usually set around ten times higher than the sampling time [29].

If this time constant is considerably higher than the outer control loops, for the sake of small-signal analysis it can be safely assumed that d and q-axis currents instantaneously follow their references. Since only active power exchange with the grid is considered in this application, the reference for q-axis is always set to zero, and solely the contribution of d-axis current will appear in the DC link current expression:

$$i_{grid} = 1.5\frac{v_d i_d}{v_{DC}} \tag{4}$$

with v_{DC} being the common DC link voltage, v_d the voltage on converter terminals at the common DC link side expressed in synchronous reference frame and i_d the d-axis current.

One can linearize (4) around the operating common DC voltage V_{DC} and obtain the following expression:

$$\hat{i_{grid}} = 1.5\frac{(e_d + 2\,I_d\,R_{line} + I_d\,L_{line}\,s)}{V_{DC}}\hat{i_d} \tag{5}$$

Where I_d is the equilibrium value of i_d. The reference for i_d is generated by the upper control layer, the principle of which is presented in Section III.

It is worth of notice that the model of the converter may be easily expanded so as to incorporate a complete LCL filter configuration. This is done by decomposing the filter into two parts; grid-side LC and converter side L filter. In that case, e_q and e_d should be replaced with the LC filtered voltage from the grid [30]. In this paper, for simplicity, a single L stage has been used for the GC.

C. Flywheel Energy Storage System

Flywheel ESS can be modeled as an additional inertia connected to the shaft of the IM. Therefore, in order to obtain a complete model of this subsystem, it remains only to model the IM and associated control loops. A set of differential equations describing the motion of an IM in field coordinates is given as follows [32]:

$$\begin{bmatrix}\dot{i_d}\\ \dot{i_q}\end{bmatrix} = \frac{v_{DC}}{\sigma L_s}\begin{bmatrix}d_d\\ d_q\end{bmatrix} + \begin{bmatrix}-\frac{R_s}{\sigma L_s} & \omega_{mR}\\ -\omega_{mR} & -\frac{R_s}{\sigma L_s}\end{bmatrix}\begin{bmatrix}i_d\\ i_q\end{bmatrix} - \frac{1}{\sigma L_s}\begin{bmatrix}0\\ \omega_{mR}\psi_r\frac{L_0}{L_r}\end{bmatrix} \tag{6}$$

where L_s, L_r, R_s, R_r are stator and rotor inductances and resistances, respectively and L_0 is the mutual inductance; i_d and i_q d and q-axis currents in field coordinates, ω_{mR} is the flux rotational speed, i_{mR} is the magnetizing current, while ψ_r is the rotor flux; σ is the total leakage coefficient, defined as

$$\sigma = 1 - \frac{1}{(1+\sigma_s)(1+\sigma_r)}, \tag{7}$$

where

$$\sigma_s = 1 - \frac{L_s}{L_0}, \sigma_r = 1 - \frac{L_r}{L_0}. \tag{8}$$

The magnetizing current i_{mR} and i_d are related with

$$L_r\frac{di_{mR}}{dt} = R_r(i_d - i_{mR}), \tag{9}$$

while the link between field and rotor orientation is given by

$$\omega_{mR} = \omega_{rot} + \frac{R_r i_q}{L_r i_{mR}} \tag{10}$$

where ω_{rot} is the rotational speed of the rotor.

Using the equivalent design principle for the inner control loops as in the case of grid rectifier, one may cancel the nonlinearity in the first term of (6) by applying feed-forward terms, setting the parameters of current PI controllers so as to cancel the $\sigma L_s \cdot s + R_s$ pole and dividing its output with v_{DC}. Then, it can be assumed that IM will follow the imposed current references with only a first order delay. Furthermore, if the corresponding time constant is considerably lower than those of other controllers, which is normally the case, it is reasonable to neglect it in small signal analysis.

The flywheel current flowing towards the common DC bus may be expressed as

$$i_{fly} = 1.5\frac{v_d i_d + v_q i_q}{v_{DC}}. \tag{11}$$

Substituting (6) into (11) and performing some manipulations using (7)-(10), the objective of which is to isolate the rotor speed term in the DC link current, one may linearize the resulting expression around V_{DC} and obtain

$$\hat{i_{fly}} = 1.5\frac{2\left(R_s + \left(\frac{L_0}{Lr}\right)^2 R_r\right) I_q + \frac{\omega_{rot0}L_0^2 I_d}{L_r} + \sigma L_s I_q s}{V_{DC}}\hat{i_q}, \tag{12}$$

where I_q, I_d are the equilibrium values for currents in field coordinates, whereas ω_{rot0} is the instantaneous rotational speed. It is worth noticing that $\hat{\omega_{rot}}$ was neglected in this small signal expression due to high flywheel inertia which makes its dynamics decoupled from the rest of the system. Moreover, $\hat{i_d}$ was neglected since rotor time constant prevents its rapid changes, while controls maintain its steady state value constant in the normal operating mode when the machine is magnetized [32].

The swing equation of the flywheel governs the changes in the rotational speed of the rotor

$$J\frac{d\omega_{rot}}{dt} = T_{el}, \tag{13}$$

where J is the flywheel inertia, while T_{el} is the electrical torque of the machine defined as

$$T_{el} = 1.5p(1-\sigma)L_s i_{mR} i_q, \tag{14}$$

with p being the number of pole pairs. Notice that is no mechanical load attached to the flywheel as its sole purpose is to store the energy.

III. Fast Charging Station Supervisory Control

The task of the FCS supervisory control is to coordinate the operation of grid connected rectifier and flywheel in the presence of HEV chargers that are connected directly to the common DC bus. Its main purpose is to reduce the impact of a sudden current step caused by HEV charger on utility with the help of energy stored in flywheel.

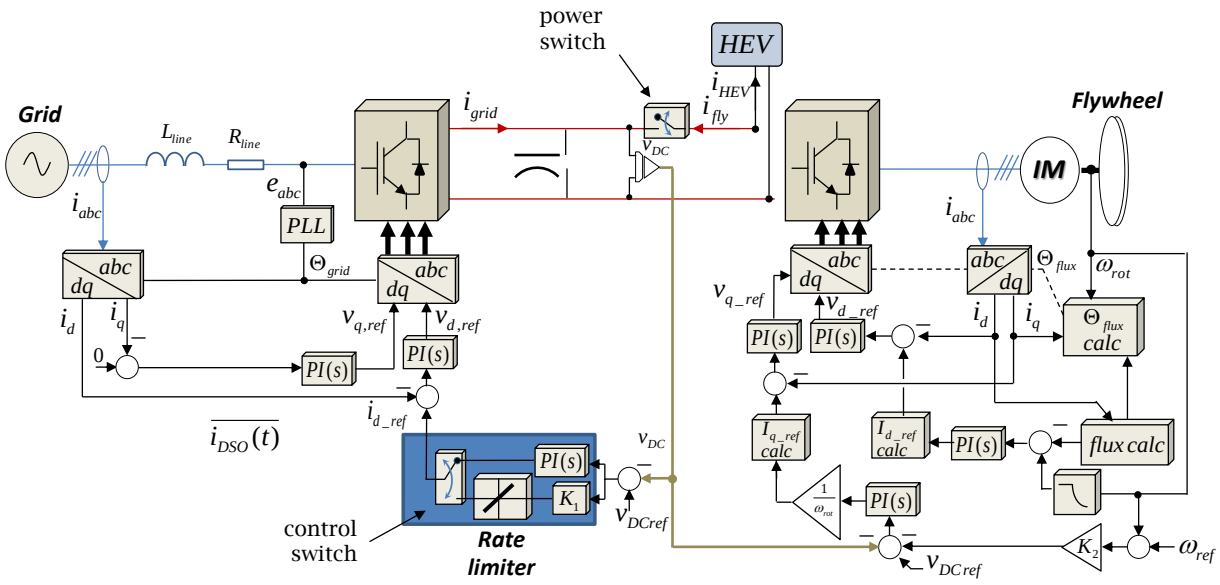

Fig. 2. Flywheel and grid converter control schemes (upper positions of power and control switches correspond to conventional FCS topology).

A. Control Objectives

The allocation of the energy stored in flywheel in this application is to counterbalance the high power extraction from HEV charger in the moment of connection and after on. In that sense, if the GC is controlled to slowly increase its power injection into the FCS, the interconnected power system may be spared from quick current steps that reduce its effective spinning reserve.

On the other hand, it is desirable that the operation of the system does not rely on any critical centralized communications which may entail problems such as single point of failure and difficult expandability. However, since the common bus voltage is generally jointly regulated by a number of converters using decentralized control systems, the design of associated controllers is dependent on each other. For that matter, once the control strategy is defined, it is essential to develop a model that is able to capture the dominant dynamics of the system in order to check its stability properties over a range of controller set parameters and operating conditions.

In accordance with the foregoing discussion, following control objectives are underlined as crucial for deployment of flexible FCS supervisory control:

- Design decentralized control strategy which makes the flywheel automatically supplying the initial power peak of HEV charger and limits the rate of grid current increase.
- Ensure that flywheel is fully recharged following the transient and that common DC voltage is restored to the nominal value.
- Calculate the flywheel energy requirements for reliable implementation of proposed strategy.
- Develop a stability representation of the system that captures its dominant dynamics. Accordingly select proper control parameters and ensure that rate limiter does not introduce limit cycles.

First three items are elaborated in subsections below, whereas the fourth one is treated in Section IV.

B. Proposed Control Strategy

The complete control diagram of the system is depicted in Fig. 2. One may notice two switches in the figure which are shown in order to clearly distinguish the conventional FCS and proposed topology (determined by position of power switch) with associated control circuit modifications (control switch).

In that sense, upper position of both switches gives the conventional structure which will not be elaborated in detail since it doesn't require any coordination strategy and operation of such a system is well understood [29]. Nevertheless, the simulation results corresponding to it are included in Section V in order to compare its performance with proposed strategy, which becomes active by putting both switches in the bottom position. The supervisory control in this case operates in distributed fashion, on top of inner regulation loops of GC and FC. Unlike using dedicated communication for coordination between the two, herein a common DC voltage is used as the sole communication medium. Hence, it can be stated that this strategy falls under the category of DBS management methods, which were originally proposed for distributed control of DC microgrids.

The strategy was designed to simultaneously satisfy all requirements imposed in the first and second item of previous subsection. In that sense, the common DC voltage variations driven by a sudden connection of HEV charger were used to govern the currents given by GC and FC. It was necessary to implement two voltage controllers that operate in parallel, and consequently the application of stiff voltage regulation was not suitable. In accordance with that and knowing that energy stored in flywheel is a function of its rotational speed, an ω_{rot} vs. v_{DC} droop has been installed on top of FC voltage

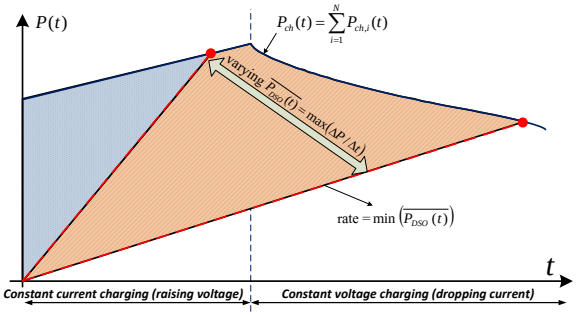

Fig. 3. Sketch of the HEV power during the execution of the fast charging algorithm paired with varying time-signal from DSO that define permitted rate of change for power extraction from the grid.

controller. On the other hand, the voltage controller of GC was designed as a proportional gain followed by the rate limiter.

Observing the overall hierarchical control structure, one can get an impression of the system's reaction to the sudden HEV charger connection, even without an explicit solution to all state equations. To that end, the response of a properly tuned system can be divided into several stages;

1) DC voltage dip caused by the HEV charger will saturate the rate limiter in GC and all the power will be provided by the FC, causing the reduction in its rotational speed.
2) After the initial dip, the common DC voltage recovers to a value specified by ω_{rot} vs. v_{DC} droop. Therefore, grid current continues to increase according to the rate limiter, which will remain saturated if the proportional gain in GC voltage controller is set high enough.
3) At a certain point, the grid current equalizes with and exceeds the HEV charging current. Since the difference between these two currents flows into flywheel, its rotational speed begins to increase, implying also the correlated rise of the common DC voltage.
4) As deviation of the common DC voltage gets reduced, rate limiter becomes unsaturated and GC starts to reduce its current up to the point where there is no deviation (GC current is then equal to those of HEV). In this condition the flywheel is fully recharged and voltage of DC bus is at nominal value.

C. Flywheel Inertia Calculation

A typical power profile in case of fast charging for the HEV is indicated by the upper boundary line in Fig. 3 [17]. One may observe that the profile is divided into two principal stages; first one is characterized by a constant current and rising voltage (power rising nearly linearly), whereas the second one by constant voltage and descending current (decreasing power).

According to the strategy proposed in previous subsection, flywheel will first have to compensate for initial peak power of HEV and then for its decreasing share, until the moment when GC current equalizes with those of HEV. Therefore, the flywheel energy demand for this application can be defined as an area surrounded by the upper boundary and the line that indicates the maximum permissible slope of GC. Fig. 3 shows that this area may change according to real-time rate limitation commands from the DSO, denoted by $\overline{P_{DSO}(t)}$ and expressed in W/s. However, looking back at Fig. 2, it can be seen that the rate limiter block ramps d-axis current component, rather than power. Therefore, the power rate should be mapped to current rate with the following relation

$$\overline{i_{DSO}(t)} = \frac{\overline{P_{DSO}(t)}}{1.5 \cdot v_d}. \tag{15}$$

The energy calculation should be done in accordance to slowest possible rate limitation which the DSO agrees not to violate. It results in the maximum area in Fig. 3 and can be expressed as

$$rate = min(\overline{P_{DSO}(t)}). \tag{16}$$

Except for the minimum rate limit, it is also necessary to take into account the typical charging profiles of HEVs for which the station is designed for. For that matter, as a basis for analysis, it is safe to use the worst case scenario where all the plugs within the station get connected at the same time by empty HEVs. Then, maximum possible area determined by the latter corresponds to the energy required by flywheel. It may be calculated as

$$E_{fly} = \int_0^{\Delta T} \sum_{i=1}^{N} P_{ch,i}(t)dt - rate \cdot \Delta T. \tag{17}$$

where $P_{ch,i}(t)$ is the instantaneous charging power of i^{th} HEV and ΔT is the period from beginning of charging until the point of intersection between GC and aggregated HEV powers. Using the data for combined charging pattern of all HEVs, ΔT may be calculated numerically via the following equation

$$\sum_{i=1}^{N} P_{ch,i}(\Delta T) = rate \cdot \Delta T. \tag{18}$$

The energy stored in flywheel is directly related to the total inertia attached to its shaft. Thus, taking into account the conservative calculation of energy in (17), the minimum required inertia may be derived as

$$J_{min} = 2\frac{E_{fly}}{\omega_{rot}^2}. \tag{19}$$

It should be noticed that actual J will be in general selected to a somewhat higher value than suggested by (19) since flywheel has to supply electrical and mechanical losses in the system during the transient. Furthermore, design should be made flexible enough to handle any unforeseen expansions in terms of connecting additional HEVs and to avoid very low rotational speeds. For that reasons, J in this paper has been selected to approximately 2.5 times higher value than predicted by J_{min} calculation.

IV. Small-Signal Stability Analysis

A small-signal analysis was used to investigate the stability and transient response of the system with deployed DBS strategy. For that matter, the small-signal models of GC and FC presented in (5) and (12) were combined with the loops

$$(C_{DC} + g_{2p}k_{pq} + K_1 g_{1p})\, s^3 - (FK_1K_2 g_{1p}k_{pq} - K_1 g_{1i} - g_{2p}k_{iq} - g_{2i}k_{pq} + C_{DC}FK_2k_{pq})\, s^2 \\ -(C_{DC}FK_2k_{iq} + FK_1K_2g_{1p}k_{iq} + FK_1K_2g_{1i}k_{pq} - g_{2i}k_{iq})s - FK_1K_2g_{1i}k_{iq} = 0 \quad (18)$$

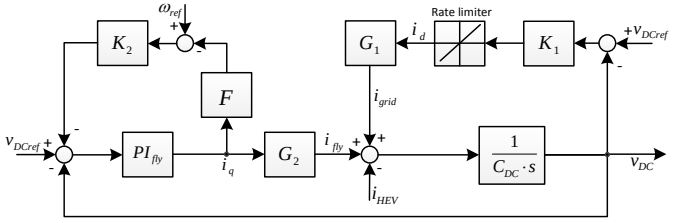

Fig. 4. Small-signal model of FCS.

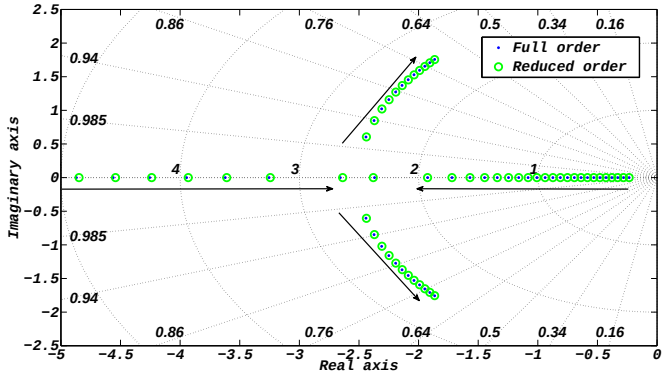

Fig. 5. Root locus of the dominant poles of (18) and poles of (21) where arrows indicate K_1 increasing from 0.5 to 4 in steps of 0.1.

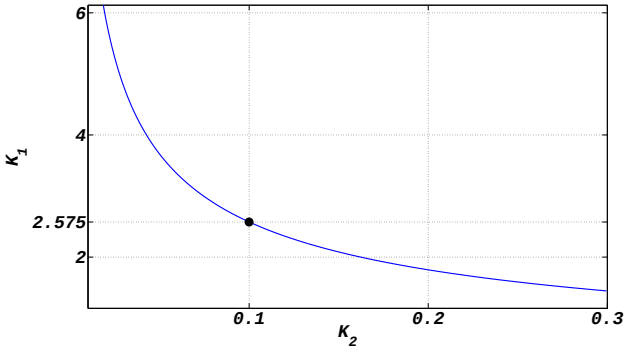

Fig. 6. Selection of optimal values for K_1 and K_2.

belonging to upper control layer (see Fig. 2), resulting in a block diagram shown in Fig. 4. In the respective figure G_1 and G_2 denote the transfer functions from i_d and i_q to i_{grid} and i_{fly}, which can be expressed as $G_1 = g_{1d} \cdot s + g_{1p}$ and $G_2 = g_{2d} \cdot s + g_{2p}$, respectively. K_1 and K_2 indicate the proportional term of the voltage controller in GC and droop coefficient in FC, respectively. F represents the machine's swing equation, while PI_{fly} is the FC voltage controller, defined as $k_{pq} + k_{iq}/s$.

A. Reduced Order Model

Taking into account complete representations of all transfer functions in the model, a third order characteristic equation may be derived, as shown in (18) at the top of next page. However, if parameter values used for the real-time simulation platform are included (see Table I), one may notice that terms g_{1p} and g_{2p} are several orders of magnitude lower than other terms, virtually canceling all their multiplicands. If this terms are neglected, and recognizing also that C_{DC}, which then remains the sole multiplicand of s^3, is much smaller than other terms, one may simplify (18) to a second order system of the following form

$$s^2 - s\frac{(C_{DC}\, F\, K_2\, k_{iq} - g_{2i}\, k_{iq} + F\, K_1\, K_2\, g_{1i}\, k_{pq})}{K_1\, g_{1i} + g_{2i}\, k_{pq} - C_{DC}\, F\, K_2\, k_{pq}} \\ -\frac{F\, K_1\, K_2\, g_{1i}\, k_{iq}}{K_1\, g_{1i} + g_{2i}\, k_{pq} - C_{DC}\, F\, K_2\, k_{pq}} = 0. \quad (21)$$

The justification of these simplifications can be found in the comparison between the dominant poles of (18) and (21). For that purpose, parameter K_1 has been selected for the sweep using values from 0.5 to 4. With all other parameters being chosen as in Table I, the root locus results are shown in Fig. 5. Since the dominant poles practically overlap in the region of interest, (21) can be used to determine the set of parameters that will lead the system to a desired damping.

It should be noted that dominant poles in the figure are associated with the response of flywheel rotational speed and hence also the common DC voltage since they are coupled by the droop law. Thus, it is desirable that the system damping is equal to 1 since the flywheel recharge then takes place in the optimal way. The most influential parameters that specify the shape of the response are K_1 and K_2, and hence their values need to be harmonized. To that end, (21) was used to calculate the relationship between those two parameters for damping equal to 1, and the result was plotted in Fig. 6. The selection of a concrete point on the plotted line was based on restrictions of droop gain, K_2. Too large value in that sense would cause unnecessarily big voltage deviations, whereas too small value could make the deviation too small and jeopardize the reliability of its detection. Value of 0.1 has hence been chose as a trade-off.

It should be noted that the characteristic equation is derived on the premise that the rate limiter in GC controller does not impact the dynamics of the system in the sense that it does not introduce oscillations during transitions between saturated and unsaturated mode. Therefore, an analytical proof for the absence of limit cycles is carried out in the following subsection.

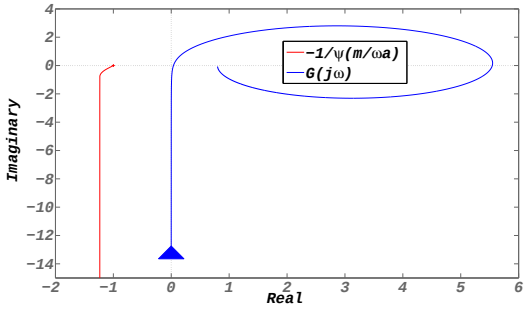

Fig. 7. Nyquist diagram for G(jω) and $-\frac{1}{\psi(m/\omega a)}$.

B. Analysis of Rate Limiter

Rate limiter is referred to as a hard non-linearity, which means that it is discontinuous and hence cannot be locally approximated by the linear function. On the other hand, the impact of rate limiter can be studied with the describing function (DF) method. The basic idea behind it is to determine ψ, which is the analytical relationship between a fictitious sinusoidal signal at the input and the output of the non-linearity, and plot its negative inverse on Nyquist plot alongside the transfer function of the corresponding linear system, $G(j\omega)$. If there exist an intersection between the two lines, with none of the points on ψ after intersection being encircled by $G(j\omega)$, there also exist a stable limit cycle [37].

Describing function for rate limiter has been developed in [38] and the same principle was applied in this paper. This non-linearity has three modes of operation; saturated, unsaturated and alternating mode. It can be shown that the negative inverse Nyquist plots in all of this modes build on each other, resulting in a continuous line that lies in the third quadrant, as shown in Fig. 7. The same figure also shows the Nyquist plot of $G(j\omega)$, which always stays in the first and fourth quadrant. Therefore, rate limiter will not introduce limit cycles in this system.

V. Simulation Results

Full model of the plant, as presented in Fig. 2 was assembled in Matlab/Simulink and compiled into dSPACE 1006. The parameters used for study may be found in Table I. Simulation of the moment of connection of HEV to the charging station has been performed for two case scenarios. First one was done using conventional topology, i.e. without a dedicated ESS for compensation of initial power peak. In that situation, the proportional voltage controller with gain K_1 was replaced with a PI whose parameters can be found at the bottom of Table I. Connection of HEV(s) was designed to occur at 3.5 seconds and the current extracted by it is represented by signal i_{HEV}. As elaborated previously, it should be noted that without the loss of generality, i_{HEV} can represent the power extraction of a single or aggregated number of vehicles. In order to demonstrate the performance of the system in both recharging stages in reduced simulation time, the capacity of the HEV's battery was down-scaled to $0.2Ah$.

TABLE I
Real-time Simulation Setup Parameters

Parameter	Value
Electrical parameters	
C_{DC}	$2.2mF$
L_{line}	$3.8mH$
R_{line}	0.24Ω
$V_{grid}(p-p)$	$325V$
HEV	
T_{HEV}	$0.02s$
$Capacity$	$0.2Ah$
Induction machine	
L_0	$10.46mH$
L_s	$10.76mH$
L_r	$10.76mH$
R_s	0.0148Ω
R_r	0.0093Ω
σ	0.055
J	10 kgm^2
Flywheel control	
T_{fly}	$0.00025s$
kp_q	3
ki_q	100
ω_{ref}	$1500rpm$
K_2	0.1
Grid rectifier control with ESS	
T_{grid}	$0.00025s$
K_1	2.575
i_{drate}	$25A/s$
Grid rectifier control without ESS	
T_{grid}	$0.00025s$
kp_d	3
ki_d	100

For the second case scenario, permitted rate limit for i_d current of GC was set to $25A/s$, which is a somewhat higher value than expected in practical applications. This is also for speeding up the effective simulation time. Simulation was performed for one full discharge/charge cycle of the flywheel ESS following the connection of HEV(s) at 3.5 seconds. In order to comply with the decentralized control principle, feed-forward compensation of HEV current, which could significantly reduce the initial voltage dip, was not applied to FC. However, since the speed of HEV charger is generally much lower ($T_{HEV} = 0.2s$ in this paper) than those of FC outer controller, the respective dip is not a critical issue. The charging profile of the HEV battery model explained in Section II-A was captured to calculate the minimal required flywheel inertia using (19). After multiplying the obtained value with 2.5, $J \approx 10kgm^2$ was derived.

Propagation of respective DC currents and DC voltage for both case scenarios are shown in the same figures in order to clearly demonstrate the differences in their performances. Fig. 8 shows the propagation of DC currents. It can be seen that the HEV current in case of conventional topology is fully compensated by the GC, introducing a current shock for the distribution grid. Quick restoration of common DC voltage following HEV connection, governed by a stiff PI voltage regulator, is observed in Fig. 9.

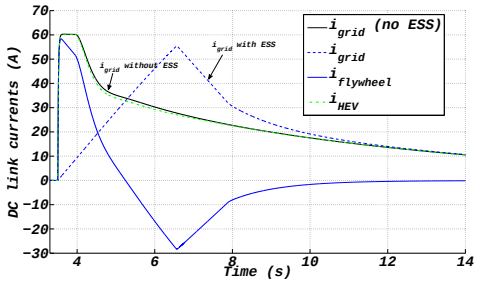

Fig. 8. DC current propagation throughout the transient.

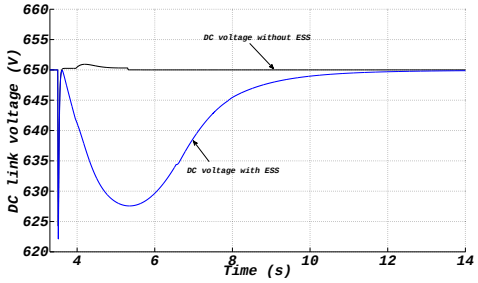

Fig. 9. Common DC voltage propagation throughout the transient.

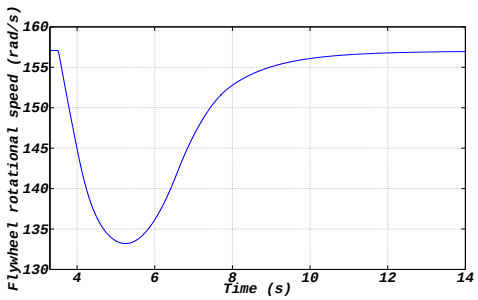

Fig. 10. Flywheel speed propagation throughout the transient.

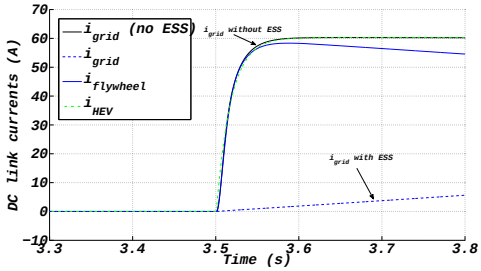

Fig. 11. Flywheel, grid converter and HEV currents following start of charging.

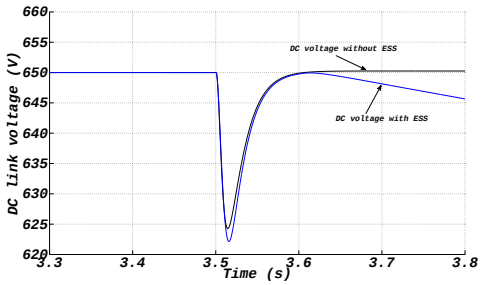

Fig. 12. Common DC voltage following start of charging.

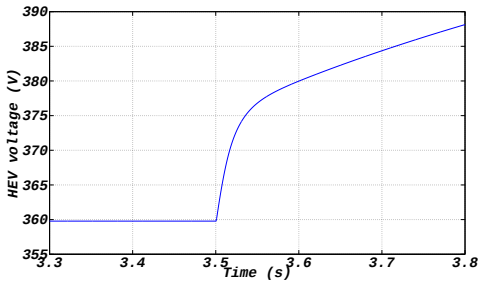

Fig. 13. HEV battery voltage following start of charging.

On the other hand, with dedicated ESS installed, FC compensates for initial HEV current, while GC operates in rate saturated mode and slowly increases its current. In that sense, flywheel acts as a power shock absorber. After the sum of HEV and FC current equalize with those of GC, it exits the saturated mode and starts regulating the common DC voltage, eventually reaching the steady state value of 650 V (while at the same time recharging the flywheel). Fig. 10 shows the full propagation of flywheel rotational speed from the starting moment of HEV charging ($t = 3.5s$), until the its full recharge.

Zoomed-in capture of the moment of HEV connection for both cases is given in Figs. 11 and 12. Fig 13 shows the propagation of HEV battery voltage derived from the model elaborated in Section II-A.

Simulation results performed on a full scale non-linear model of the plant show the effectiveness of deploying flywheel ESS to serve as a shock absorber in FCS applications. When compared to conventional control method which has a stiff PI voltage regulator implemented within GC, a cost of decentralized coordination can be seen in slow restoration of common DC link voltage since it is directly linked via droop with rotational speed of the flywheel. Although not critical, this obstacle may be easily resolved with use of low bandwidth communication, which still presents a progress with respect to previously proposed methods which rely on high bandwidth communication between GC and FC. Response of the proposed strategy showed good agreement with the control design performed on a reduced order linear model. It can be seen that the flywheel is able to provide the initial transient of current and get fully recharged without any oscillations, as predicted by reduced order model.

VI. Conclusion

In this paper, a power balancing strategy for the FCS has been proposed. It takes into account both the retention of vehicle owners' comfort level in terms of providing quick battery recharge time and a grid-friendly propulsion. The power balancing feature was realized by means of a novel DBS control method that relies on a low-speed flywheel ESS. Developed strategy was analyzed in detail for charging only

one HEV, but it can be easily expanded to support a number HEVs due to dynamic characteristics of typical HEV chargers. Also the inclusion of additional ESS is greatly facilitated by distributed nature of proposed control principle. In that sense, a number of ESS can operate in parallel if each one of them operates in a voltage droop control mode. This expandability feature is within the scope of author's current research work.

For the purpose of tuning the control parameters of the system, a reduced order small signal stability model has been assembled. It showed good agreement with the complete non-linear model of the plant in the operating range of interest. Moreover, it has been used to analytically prove that the rate limiter will not introduce any limit cycles. Finally, real-time simulation results that compare the responses of conventional system and proposed one have been presented to verify the validity of novel control method.

REFERENCES

[1] A. Saber and G. Venayagamoorthy, "Plug-in vehicles and renewable energy sources for cost and emission reductions," *Ind. Electron., IEEE Trans. on*, vol. 58, no. 4, pp. 1229–1238, 2011.

[2] X. Chang, B. Chen, Q. Li, X. Cui, L. Tang, and C. Liu, "Estimating real-time traffic carbon dioxide emissions based on intelligent transportation system technologies," *Intelligent Transportation Syst., IEEE Trans. on*, vol. 14, no. 1, pp. 469–479, 2013.

[3] S. Kobayashi, S. Plotkin, and S. K. Ribeiro, "Energy efficiency technologies for road vehicles," *Energy Efficiency*, vol. 2, no. 2, pp. 125–137, 2009.

[4] M. Ehsani, Y. Gao, and A. Emadi, *Modern Electric, Hybrid Electric, and Fuel Cell Vehicles: Fundamentals, Theory, and Design, Second Edition*. Power Electron. and Appl. Series, Taylor & Francis, 2009.

[5] Z. Fan, "A distributed demand response algorithm and its application to phev charging in smart grids," *Smart Grid, IEEE Trans. on*, vol. 3, no. 3, pp. 1280–1290, 2012.

[6] A. Rautiainen, S. Repo, P. Jarventausta, A. Mutanen, K. Vuorilehto, and K. Jalkanen, "Statistical charging load modeling of phevs in electricity distribution networks using national travel survey data," *Smart Grid, IEEE Trans. on*, vol. 3, no. 4, pp. 1650–1659, 2012.

[7] D. Steen, L. Tuan, O. Carlson, and L. Bertling, "Assessment of electric vehicle charging scenarios based on demographical data," *Smart Grid, IEEE Trans. on*, vol. 3, no. 3, pp. 1457–1468, 2012.

[8] M. Yilmaz and P. Krein, "Review of battery charger topologies, charging power levels, and infrastructure for plug-in electric and hybrid vehicles," *Power Electron., IEEE Trans. on*, vol. 28, no. 5, pp. 2151–2169, 2013.

[9] J. Machowski, J. W. Bialek, and J. R. Bumby, *Power System Dynamics: Stability and Control*. John Wiley-Sons, Ltd, 2008.

[10] K. Clement-Nyns, E. Haesen, and J. Driesen, "The impact of charging plug-in hybrid electric vehicles on a residential distribution grid," *Power Syst., IEEE Trans. on*, vol. 25, no. 1, pp. 371–380, 2010.

[11] K. Qian, C. Zhou, M. Allan, and Y. Yuan, "Modeling of load demand due to ev battery charging in distribution syst.," *Power Syst., IEEE Trans. on*, vol. 26, no. 2, pp. 802–810, 2011.

[12] D. Wu, D. Aliprantis, and K. Gkritza, "Electric energy and power consumption by light-duty plug-in electric vehicles," *Power Syst., IEEE Trans. on*, vol. 26, no. 2, pp. 738–746, 2011.

[13] U. Madawala and D. Thrimawithana, "A bidirectional inductive power interface for electric vehicles in v2g syst.," *Ind. Electron., IEEE Trans. on*, vol. 58, no. 10, pp. 4789–4796, 2011.

[14] E. Sortomme and M. El-Sharkawi, "Optimal scheduling of vehicle-to-grid energy and ancillary services," *Smart Grid, IEEE Trans. on*, vol. 3, no. 1, pp. 351–359, 2012.

[15] "European Technology Platform SmartGrids: Strategic Research Agenda: Update of the SmartGrids SRA 2007 for the needs by the year 2035." http://www.smartgrids.eu/documents/sra2035.pdf, 2012. [Online; accessed 13-October-2013].

[16] H. Hoimoja, A. Rufer, G. Dziechciaruk, and A. Vezzini, "An ultrafast ev charging station demonstrator," in *Power Electron., Electrical Drives, Automation and Motion (SPEEDAM), 2012 International Symposium on*, pp. 1390–1395, 2012.

[17] S. Bai and S. Lukic, "Unified active filter and energy storage system for an mw electric vehicle charging station," *Power Electron., IEEE Trans. on*, vol. 28, no. 12, pp. 5793–5803, 2013.

[18] D. Linden and T. B. Reddy, *Handbook of Batteries*. McGraw-Hill, 2002.

[19] J. Barton and D. Infield, "Energy storage and its use with intermittent renewable energy," *Energy Convers., IEEE Trans. on*, vol. 19, pp. 441–448, June 2004.

[20] C. Abbey and G. Joos, "Supercapacitor energy storage for wind energy appl.," *Ind. Appl., IEEE Trans. on*, vol. 43, pp. 769–776, May 2007.

[21] S. Vazquez, S. Lukic, E. Galvan, L. Franquelo, and J. Carrasco, "Energy storage syst. for transport and grid appl.," *Ind. Electron., IEEE Trans. on*, vol. 57, no. 12, pp. 3881–3895, 2010.

[22] H. Akagi and H. Sato, "Control and performance of a doubly-fed induction machine intended for a flywheel energy storage system," *Power Electron., IEEE Trans. on*, vol. 17, no. 1, pp. 109–116, 2002.

[23] R. Cardenas, R. Pena, G. Asher, J. Clare, and R. Blasco-Gimenez, "Control strategies for power smoothing using a flywheel driven by a sensorless vector-controlled induction machine operating in a wide speed range," *Ind. Electron., IEEE Trans. on*, vol. 51, no. 3, pp. 603–614, 2004.

[24] S. Samineni, B. Johnson, H. Hess, and J. Law, "Modeling and analysis of a flywheel energy storage system for voltage sag correction," *Industry Appl., IEEE Trans. on*, vol. 42, no. 1, pp. 42–52, 2006.

[25] G. Cimuca, C. Saudemont, B. Robyns, and M. Radulescu, "Control and performance evaluation of a flywheel energy-storage system associated to a variable-speed wind generator," *Ind. Electron., IEEE Trans. on*, vol. 53, no. 4, pp. 1074–1085, 2006.

[26] J. Schonberger, R. Duke, and S. Round, "DC-Bus Signaling: A Distributed Control Strategy for a Hybrid Renewable Nanogrid," *IEEE Trans. on Ind. Electron.*, vol. 53, pp. 1453–1460, Oct. 2006.

[27] K. Sun, L. Zhang, Y. Xing, and J. M. Guerrero, "A Distributed Control Strategy Based on DC Bus Signaling for Modular Photovoltaic Generation Syst. With Battery Energy Storage," *IEEE Trans. on Power Electron.*, vol. 26, pp. 3032–3045, Oct. 2011.

[28] T. Dragicevic, J. Guerrero, J. Vasquez, and D. Skrlec, "Supervisory control of an adaptive-droop regulated dc microgrid with battery management capability," *Power Electron., IEEE Trans. on*, vol. 29, no. 2, pp. 695–706, 2014.

[29] V. Blasko and V. Kaura, "A new mathematical model and control of a three-phase ac-dc voltage source converter," *Power Electron., IEEE Trans. on*, vol. 12, no. 1, pp. 116–123, 1997.

[30] V. Blasko and V. Kaura, "A novel control to actively damp resonance in input lc filter of a three-phase voltage source converter," *Industry Appl., IEEE Trans. on*, vol. 33, no. 2, pp. 542–550, 1997.

[31] M. Liserre, F. Blaabjerg, and S. Hansen, "Design and control of an lcl-filter-based three-phase active rectifier," *Industry Appl., IEEE Trans. on*, vol. 41, no. 5, pp. 1281–1291, 2005.

[32] W. Leonhard, *Control of Electrical Drives, Third edition*. Power Syst., Springer, 2001.

[33] T. Dragicevic, *Hierarchical Control of a Direct Current Microgrid with Energy Storage Syst. in a Distributed Topology*. PhD Thesis, 2013.

[34] J. Cao and A. Emadi, "Batteries need electron.," *Ind. Electronics Magazine, IEEE*, vol. 5, no. 1, pp. 27–35, 2011.

[35] M. Chen and G. Rincon-Mora, "Accurate Electrical Battery Model Capable of Predicting Runtime and IV Performance," *IEEE Trans. on Energy Convers.*, vol. 21, pp. 504–511, June 2006.

[36] "2013 Chevrolet Volt VIN 3929 Advanced Vehicle Testing Beginning-of-Test Battery Testing Results." http://www1.eere.energy.gov/vehiclesandfuels/avta/pdfs/phev/battery_volt_3929.pdf, 2013. [Online; accessed 30-September-2013].

[37] J. Slotine and W. LI, *Applied Nonlinear Control*. Prentice Hall, 1991.

[38] F. Gordillo, I. Alcal, and J. Aracil, "Bifurcations in syst. with a rate limiter," in *Dynamics, Bifurcations, and Control* (F. Colonius and L. Grne, eds.), vol. 273 of *Lecture Notes in Control and Information Sciences*, pp. 37–50, Springer Berlin Heidelberg, 2002.